Terahertz Spin-Current Pulses from an Off-Resonant Antiferromagnet

Chi Sun,[1,2,*] Hyunsoo Yang,[1] Arne Brataas,[2] and Mansoor B. A. Jalil[1,†]

[1] *Department of Electrical and Computer Engineering, National University of Singapore, 117576 Singapore*
[2] *Center for Quantum Spintronics, Department of Physics, Norwegian University of Science and Technology, Trondheim NO-7491, Norway*

(Received 12 October 2021; revised 2 February 2022; accepted 10 February 2022; published 10 March 2022)

The generation of terahertz (THz) spin current is highly desired for enhancing the speed and efficiency of information manipulation by ultrafast spintronics. We develop an analytical model to investigate the coherent and pure spin-current pulses generated by spin pumping in a canted insulating antiferromagnet (AFM) system with Dzyaloshinskii-Moriya interaction (DMI). As expected, the spin pumping signal is significant at resonance. However, we also predict efficient THz spin-current transient with a magnitude comparable with that of its resonant counterparts in the much higher off-resonance THz frequency regime. Its ultrafast temporal change compensates for the suppression of the dynamic magnetization amplitudes at off-resonance. In addition, a stronger DMI field enhances the amplitude of the spin-current transient. Our results represent an efficient approach to generate coherent THz spin-current pulses based on canted AFM heterostructures without requiring a static magnetic field.

DOI: 10.1103/PhysRevApplied.17.034028

I. INTRODUCTION

The generation, manipulation, and detection of spin current are core elements of spintronics [1–6] and provide an alternative for processing and storing information in addition to conventional electronics. Furthermore, an ultrafast spin-current response can further enhance the efficiency and speed of information computation [7–9]. Therefore, one possible avenue is to combine ultrafast optics with spintronics, e.g., terahertz (THz) emitters based on magnetic-nonmagnetic metallic heterostructures driven by laser pulses [10–13]. However, optical lasers induce incoherent thermal effects in metals by heating the electrons and pose additional challenges in lowering the power consumption. Thus, for ultrafast spintronics, the excitation of coherent spin current from magnetic insulators may offer an alternative route to reduce the thermal effects further.

In spin pumping [14–16], the magnetization dynamics in a magnetic material injects a coherent and pure spin current into the adjacent layers. The magnetic material can be a magnetic insulator (e.g., YIG) that can function as an efficient spin-current source, as extensively demonstrated [15,17,18]. In conventional ferromagnetic (FM)-nonmagnetic (NM) heterostructures, the magnetization precession is driven at ferromagnetic resonance, typically a frequency of a few gigahertz. In contrast, antiferromagnetic (AFM) materials possess much higher resonance frequencies due to the extremely large exchange coupling between the spins in the sublattices, and therefore constitute promising candidates for ultrafast spintronics. Recently, spin-current generation via spin pumping has been demonstrated in uniaxial or collinear AFMs like Cr_2O_3 [19] and MnF_2 [20] at antiferromagnetic resonance (AFMR) frequency approaching the sub-THz regime (with large external magnetic fields of several tesla). Meanwhile, spin pumping has also been studied in canted AFMs (i.e., Fe_2O_3) with Dzyaloshinskii-Moriya interaction (DMI), where the inverse spin Hall voltages are detected at the low-frequency mode of the AFMR (at tens of gigahertz) [21,22]. The noncollinear configuration of canted AFMs yields a net magnetic moment, which makes it possible to combine the advantages of FM- and AFM-based spintronics.

In this work, we compute how THz magnetic field pulses cause *transient* spin currents from insulating easy-plane AFMs (e.g., Fe_2O_3) into adjacent NMs. The DMI causes a slight canting of the magnetic moments of the two AFM sublattices. As expected, the magnetization dynamics is enhanced when the magnetic material is excited at its resonant frequencies. Surprisingly, we also find the efficient generation of coherent spin-current pulses in the higher off-resonance THz regime. In this regime, there are spin-current amplitudes comparable with those of resonant counterparts in spite of the decreased dynamic magnetization amplitudes. In addition, we show that a strong DMI field enhances the spin pumping efficiency.

*e0021580@u.nus.edu
†elembaj@nus.edu.sg

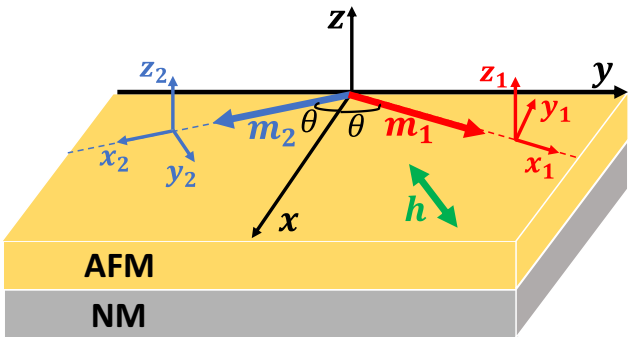

FIG. 1. The AFM/NM structure in this work. The DMI causes the two sublattice magnetizations $\mathbf{m}_1$ and $\mathbf{m}_2$ to be canted toward the x axis at an angle θ with respect to $\hat{\mathbf{x}}$ in the ground state.

II. THEORY AND MODEL

Figure 1 shows the AFM/NM structure in this work. A linearly polarized THz pulse excites the spin precession. We start by computing induced magnetization dynamics. In a macrospin approximation with two sublattices ($i = 1, 2$), the free energy of the canted AFM system is given by

$$F = \mu_0 M_s \left\{ H_E(\mathbf{m}_1 \cdot \mathbf{m}_2) + \frac{H_A}{2}[(\mathbf{m}_1 \cdot \hat{\mathbf{z}})^2 + (\mathbf{m}_2 \cdot \hat{\mathbf{z}})^2] - \frac{H_a}{2}[(\mathbf{m}_1 \cdot \hat{\mathbf{y}})^2 + (\mathbf{m}_2 \cdot \hat{\mathbf{y}})^2] + H_D \hat{\mathbf{z}} \cdot (\mathbf{m}_1 \times \mathbf{m}_2) \right\}, \tag{1}$$

where μ_0 is the vacuum permeability, $\mathbf{m}_i$ denotes the sublattice magnetization unit vector, and M_s is the saturation magnetization. Here, four field coefficients are included corresponding to the intersublattice exchange H_E, the hard-axis or easy-plane anisotropy H_A, the easy-axis anisotropy H_a, and the DMI field H_D. Note that we consider the zero-field mode, i.e., there is no external static magnetic field. Accordingly, the effective fields acting on each sublattice can be obtained from $\mathbf{H}_{\text{eff},i} = -(1/\mu_0 M_s)(\partial F/\partial \mathbf{m}_i)$ as

$$\begin{aligned} \mathbf{H}_{\text{eff},1} &= -H_E \mathbf{m}_2 - H_A(\mathbf{m}_1 \cdot \hat{\mathbf{z}})\hat{\mathbf{z}} \\ &\quad + H_a(\mathbf{m}_1 \cdot \hat{\mathbf{y}})\hat{\mathbf{y}} + H_D \hat{\mathbf{z}} \times \mathbf{m}_2, \\ \mathbf{H}_{\text{eff},2} &= -H_E \mathbf{m}_1 - H_A(\mathbf{m}_2 \cdot \hat{\mathbf{z}})\hat{\mathbf{z}} \\ &\quad + H_a(\mathbf{m}_2 \cdot \hat{\mathbf{y}})\hat{\mathbf{y}} - H_D \hat{\mathbf{z}} \times \mathbf{m}_1. \end{aligned} \tag{2}$$

In the absence of DMI, the two sublattice magnetizations align along the y axis and are antiparallel. The DMI causes $\mathbf{m}_1$ and $\mathbf{m}_2$ to be canted toward the x axis at an angle θ with respect to $\hat{\mathbf{x}}$ in the ground state (see Fig. 1). Here weak canting is considered, i.e., $H_D \ll H_E$, and therefore $\theta \approx \pi/2$.

Based on above effective fields, the magnetization dynamics is coupled by two Landau-Lifshitz-Gilbert (LLG) equations, i.e.,

$$\frac{d\mathbf{m}_i}{dt} = -\mu_0 \gamma'[\mathbf{m}_i \times \mathbf{H}_{\text{tot},i} + \alpha \mathbf{m}_i \times (\mathbf{m}_i \times \mathbf{H}_{\text{tot},i})], \tag{3}$$

where $\mathbf{H}_{\text{tot},i} = \mathbf{H}_{\text{eff},i} + \mathbf{h}(t)$ and $\mathbf{h}(t)$ is the excitation magnetic field pulse. Note $\gamma' = \gamma/(1+\alpha^2)$ with the gyromagnetic ratio γ and the damping constant α. Introducing $\{\hat{\mathbf{x}}_i, \hat{\mathbf{y}}_i, \hat{\mathbf{z}}_i\}$ as the local coordinate system for sublattice i (see Fig. 1), we express $\mathbf{m}_i = \hat{\mathbf{x}}_i + \delta\mathbf{m}_i$ with $\delta\mathbf{m}_i = m_{yi}\hat{\mathbf{y}}_i + m_{zi}\hat{\mathbf{z}}_i$ since the small-angle precession around the equilibrium magnetization direction $\hat{\mathbf{x}}_i$ is of our interest. By solving the static LLG equations, the equilibrium canting angle is obtained as $\cos\theta \approx (H_D/2H_E)$. The linearized LLG equation reads

$$\frac{d}{dt}\delta\mathbf{m} = \mathcal{M}\delta\mathbf{m} + \mathbf{F}(t), \tag{4}$$

where the vector of the dynamic magnetization components is given by $\delta\mathbf{m} = (m_{y1}, m_{z1}, m_{y2}, m_{z2})^T$. The matrices in Eq. (4) are

$$\mathcal{M} = -\mu_0\gamma' \begin{pmatrix} \alpha H_{\theta,1} & H_{\theta,2} & -\alpha H_{\theta,3} & H_E \\ -H_{\theta,1} & \alpha H_{\theta,2} & H_{\theta,3} & \alpha H_E \\ -\alpha H_{\theta,3} & H_E & \alpha H_{\theta,1} & H_{\theta,2} \\ H_{\theta,3} & \alpha H_E & -H_{\theta,1} & \alpha H_{\theta,2} \end{pmatrix}, \tag{5}$$

$$\mathbf{F}(t) = \mu_0\gamma' \begin{pmatrix} -\alpha\sin\theta & \sin\theta & \alpha\sin\theta & -\alpha\sin\theta \\ \alpha\cos\theta & -\cos\theta & \alpha\cos\theta & -\cos\theta \end{pmatrix}^T \mathbf{h}(t), \tag{6}$$

where the compact field terms $H_{\theta,1} = H_D \sin 2\theta - (H_E + H_a)\cos 2\theta$, $H_{\theta,2} = H_D \sin 2\theta + H_A + (1/2)H_a(1 - \cos 2\theta) - H_E \cos 2\theta$, and $H_{\theta,3} = H_D \sin 2\theta - H_E \cos 2\theta$ are introduced. In Eq. (6), we consider the excitation dynamic magnetic field $\mathbf{h}(t) = \mathbf{h}\exp[-([(t-t_0)^2]/2\sigma^2) + i(\Omega t + \phi_h)]$, the product of a Gaussian pulse with a width σ and temporal shift t_0 and a harmonic carrier with a frequency Ω and phase ϕ_h. Here we apply $\mathbf{h} = (h_x, h_y)^T$, i.e., the field is linearly polarized in the x-y plane (see Fig. 1). Assuming the exchange field is much larger than the other interactions, the low and high AFMR frequencies are

$$\omega_l = \mu_0\gamma'\sqrt{2H_E H_a}, \tag{7}$$

$$\omega_h = \mu_0\gamma'\sqrt{H_D^2 + 2H_E(H_A + H_a)}. \tag{8}$$

The AFMR frequencies are in the range of tens of gigahertz based on available experimental parameters for

Fe_2O_3 [21,23–25]. The corresponding complex eigenfrequencies are

$$\omega_{l(h)}^{+,-} = \pm\sqrt{\omega_{l(h)}^2 - \left(\frac{\Delta\omega}{2}\right)^2} + \frac{i\Delta\omega}{2}, \tag{9}$$

where $\Delta\omega = 2\alpha\mu_0\gamma' H_E$ is the resonance linewidth due to the Gilbert damping. In the following, we use the notation ω_j ($j = 1,2,3,4$) to represent the four eigenvalues (i.e., ω_l^+, ω_l^-, ω_h^+, and ω_h^-) for simplicity. The factor $C_j = (m_{y1}/m_{z1})$ is defined to describe the eigenvector corresponding to ω_j, where we find $C_1 = (2i\mu_0\gamma' H_E/\omega_1)$, $C_2 = (2i\mu_0\gamma' H_E/\omega_2)$, $C_3 = (i\omega_3/2\mu_0\gamma' H_E)$, and $C_4 = (i\omega_4/2\mu_0\gamma' H_E)$. Consequently, the fundamental matrix of the inhomogenous equation [i.e., Eq. (4)] constructed by the eigenpairs is expressed as

$$\mathbf{W}(t) = \begin{pmatrix} C_1 e^{i\omega_1 t} & C_2 e^{i\omega_2 t} & -C_3 e^{i\omega_3 t} & -C_4 e^{i\omega_4 t} \\ e^{i\omega_1 t} & e^{i\omega_2 t} & -e^{i\omega_3 t} & -e^{i\omega_4 t} \\ C_1 e^{i\omega_1 t} & C_2 e^{i\omega_2 t} & C_3 e^{i\omega_3 t} & C_4 e^{i\omega_4 t} \\ e^{i\omega_1 t} & e^{i\omega_2 t} & e^{i\omega_3 t} & e^{i\omega_4 t} \end{pmatrix}. \tag{10}$$

Therefore, the final analytical solution of the transient dynamic magnetization $\delta\mathbf{m}$ is given by

$$\begin{aligned} \delta\mathbf{m} &= \mathbf{W}(t)\int_0^t \mathbf{W}^{-1}(t')\mathbf{F}(t')dt' \\ &= \mu_0\gamma'\sigma\sqrt{\pi/2}\,\mathbf{W}(t)\mathbf{E}(t)\mathbf{S}h \end{aligned} \tag{11}$$

with

$$\mathbf{S} = \begin{pmatrix} 0 & 0 & \frac{(C_4+\alpha)\sin\theta}{C_3-C_4} & \frac{-(C_3+\alpha)\sin\theta}{C_3-C_4} \\ \frac{(C_2+\alpha)\cos\theta}{C_1-C_2} & \frac{-(C_1+\alpha)\cos\theta}{C_1-C_2} & 0 & 0 \end{pmatrix}^T. \tag{12}$$

The diagonal matrix $\mathbf{E}(t)$ is explicitly given by

$$\mathbf{E}(t) = \mathrm{diag}(\Delta E_1, \Delta E_2, \Delta E_3, \Delta E_4), \tag{13}$$

where $\Delta E_j = E(\omega_j, t) - E(\omega_j, 0)$ with

$$\begin{aligned} E(\omega_j, t) = \exp&\left[-\frac{\sigma^2}{2}(\omega_j - \Omega)^2 - it_0(\omega_j - \Omega) + i\phi_h\right] \\ &\times \mathrm{erf}\left[\frac{t - t_0 + i\sigma^2(\omega_j - \Omega)}{\sqrt{2}\sigma}\right]. \end{aligned} \tag{14}$$

The expression (14) involves the error function, in a similar way as derived for the dynamic magnetization transient in FM systems [26,27].

It has been proposed that spin pumping from the two sublattices of AFM constructively adds up rather than cancels [28]. Knowing the solution of $\delta\mathbf{m}$ in Eq. (9), the spin pumping current injected into the NM layer in response to the field pulse can be obtained from

$$\mathbf{I}_{\mathrm{sp}} = \frac{\hbar g_r}{4\pi}\sum_{i=1,2}\mathbf{m}_i \times \frac{d\mathbf{m}_i}{dt}, \tag{15}$$

where g_r is the spin-mixing conductance at the AFM/NM interface. Inserting $\mathbf{m}_i = \hat{\mathbf{x}}_i + \delta\mathbf{m}_i$ with $\delta\mathbf{m}_i = m_{yi}\hat{\mathbf{y}}_i + m_{zi}\hat{\mathbf{z}}_i$, $\mathbf{I}_{\mathrm{sp}}$ can be decomposed into two components as $\mathbf{I}_{\mathrm{sp}} = \mathbf{I}_{\mathrm{sp}}^{l} + \mathbf{I}_{\mathrm{sp}}^{\mathrm{nl}}$ with

$$\begin{aligned} \mathbf{I}_{\mathrm{sp}}^{l} &= \frac{\hbar g_r}{4\pi}\sum_{i=1,2}\hat{\mathbf{x}}_i \times \frac{d\delta\mathbf{m}_i}{dt} = \frac{\hbar g_r}{4\pi}\sum_{i=1,2}\left(-\frac{dm_{zi}}{dt}\hat{\mathbf{y}}_i + \frac{dm_{yi}}{dt}\hat{\mathbf{z}}_i\right) \\ &\approx \frac{\hbar g_r}{4\pi}\left[\left(\frac{dm_{z1}}{dt} - \frac{dm_{z2}}{dt}\right)\sin\theta\hat{\mathbf{x}} + \left(\frac{dm_{y1}}{dt} + \frac{dm_{y2}}{dt}\right)\hat{\mathbf{z}}\right] \end{aligned} \tag{16}$$

and

$$\begin{aligned} \mathbf{I}_{\mathrm{sp}}^{\mathrm{nl}} &= \frac{\hbar g_r}{4\pi}\sum_{i=1,2}\delta\mathbf{m}_i \times \frac{d\delta\mathbf{m}_i}{dt} \\ &= \frac{\hbar g_r}{4\pi}\sum_{i=1,2}\left(m_{yi}\frac{dm_{zi}}{dt} - m_{zi}\frac{dm_{yi}}{dt}\right)\hat{\mathbf{x}}_i \\ &\approx \frac{\hbar g_r}{4\pi}\left(m_{y1}\frac{dm_{z1}}{dt} - m_{z1}\frac{dm_{y1}}{dt} - m_{y2}\frac{dm_{z2}}{dt} + m_{z2}\frac{dm_{y2}}{dt}\right) \\ &\quad\times \sin\theta\hat{\mathbf{y}}, \end{aligned} \tag{17}$$

where $\mathbf{I}_{\mathrm{sp}}^{l}$ and $\mathbf{I}_{\mathrm{sp}}^{\mathrm{nl}}$ depend linearly and nonlinearly, respectively, on the time derivative of the dynamic magnetization. The linear (nonlinear) spin-current component polarized along $\hat{\mathbf{y}}$ ($\hat{\mathbf{x}}$), which is proportional to $\cos\theta$ ($\approx H_D/2H_E$), can be neglected in the limit of strong exchange. Therefore, $\mathbf{I}_{\mathrm{sp}}^{l}$ is composed of the in-plane and out-of-plane components polarized along $\hat{\mathbf{x}}$ and $\hat{\mathbf{z}}$, i.e., $I_{\mathrm{sp}}^{l,x}$ and $I_{\mathrm{sp}}^{l,z}$, respectively. On the other hand, $\mathbf{I}_{\mathrm{sp}}^{\mathrm{nl}}$ is purely in-plane with polarization along $\hat{\mathbf{y}}$, which is the direction of the sublattice equilibrium magnetizations. In Eqs. (16) and (17), the time derivative of the dynamic magnetization can be obtained from

$$\frac{d\delta\mathbf{m}}{dt} = \mu_0\gamma'\sigma\sqrt{\pi/2}\mathbf{W}(t)\left[i\boldsymbol{\omega}E(t) + \frac{d\mathbf{E}(t)}{dt}\right]\mathbf{S}h \tag{18}$$

with

$$\boldsymbol{\omega} = \mathrm{diag}(\omega_1, \omega_2, \omega_3, \omega_4), \tag{19}$$

$$\begin{aligned} \frac{dE(\omega_j, t)}{dt} = \frac{1}{\sigma}\sqrt{\frac{2}{\pi}}&\exp \\ &\left[-\frac{(t - t_0)^2}{2\sigma^2} - i(\omega_j - \Omega)t + i\phi_h\right]. \end{aligned} \tag{20}$$

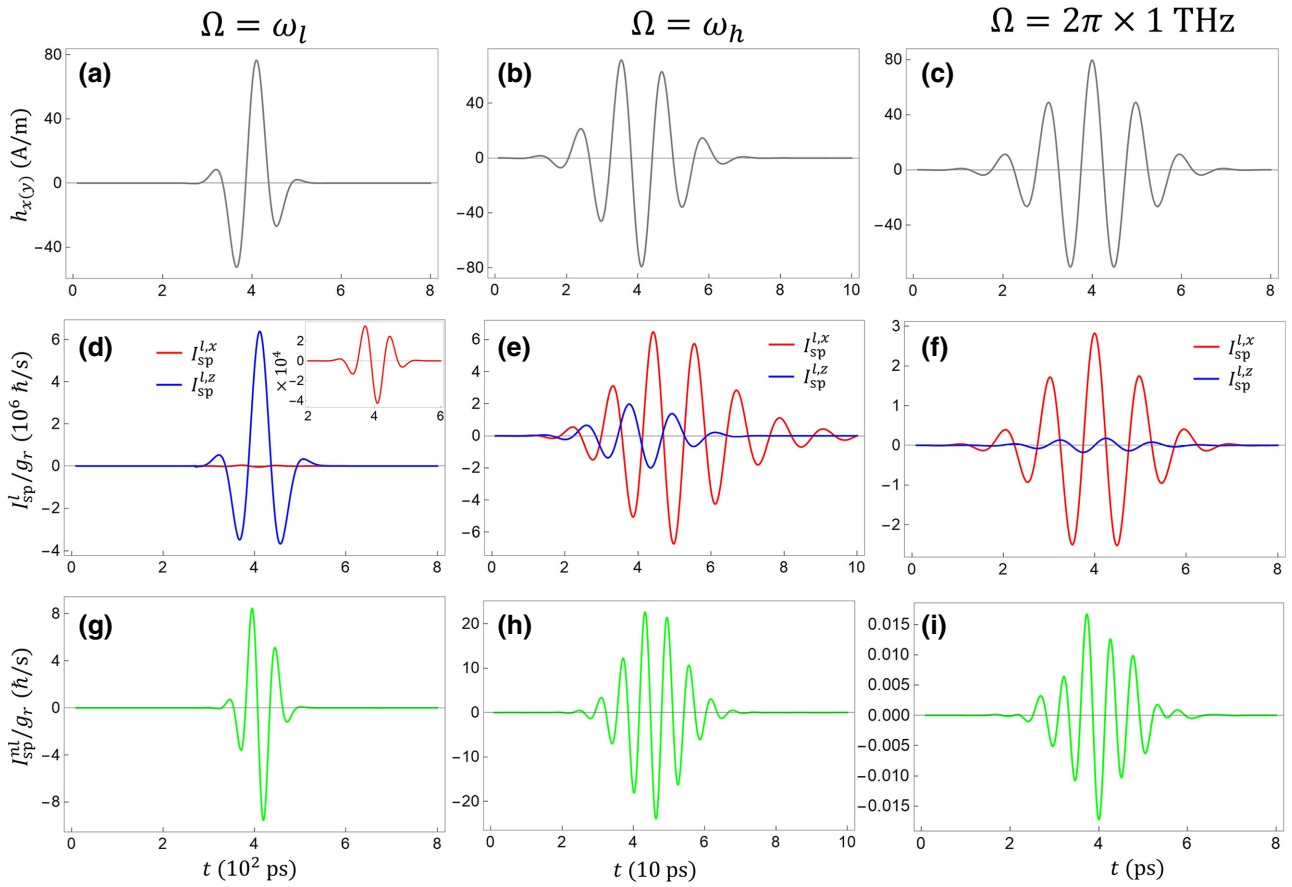

FIG. 2. Coherent spin-pumping current pulse generation excited in different ways. (a)–(c) The excitation magnetic field pulses with the two resulting spin current components $\mathbf{I}^{l}_{\rm sp}$ (d)–(f) and $\mathbf{I}^{\rm nl}_{\rm sp}$ (g)–(i) for three typical excitation frequencies, i.e., (i) $\Omega = \omega_l$, (ii) $\Omega = \omega_h$, and (iii) $\Omega = 2\pi \times 1$ THz. The red and blue lines represent the in-plane and out-of-plane polarized components of $\mathbf{I}^{l}_{\rm sp}$, i.e., $I^{l,x}_{\rm sp}$ and $I^{l,z}_{\rm sp}$, respectively. The inset in (d) gives the corresponding enlarged diagrams of the in-plane polarized $I^{l,x}_{\rm sp}$ in the main panel. In all panels, the excitation field parameters of $\mu_0 h_x = \mu_0 h_y = 0.1$ mT and $\phi_h = 0$ are assumed. Other parameters are $\sigma = 40$ ps and $t_0 = 400$ ps for case (i), $\sigma = 10$ ps and $t_0 = 40$ ps for case (ii), and $\sigma = 1$ ps and $t_0 = 4$ ps for case (iii).

III. NUMERICAL RESULTS AND DISCUSSION

The transient spin-pumping currents under three typical conditions with respect to the excitation carrier frequency are plotted in Fig. 2, i.e., (i) $\Omega = \omega_l$, (ii) $\Omega = \omega_h$, and (iii) $\Omega = 1$ THz. Here we assume material parameters corresponding to canted Fe_2O_3 [21–25], i.e., $\mu_0 H_E = 1000$ T, $\mu_0 H_A = 2 \times 10^{-3}$ T, $\mu_0 H_a = 6 \times 10^{-5}$ T, $\mu_0 H_D = 2.6$ T, and $\alpha = 4.6 \times 10^{-4}$, yielding the two AFMR frequencies at $\omega_l \sim 2\pi \times 9.7$ GHz and $\omega_h \sim 2\pi \times 85.1$ GHz. The excitation field pulses are shown with the two resulting spin-current components $\mathbf{I}^{l}_{\rm sp}$ and $\mathbf{I}^{\rm nl}_{\rm sp}$ for the three typical excitation frequencies, in the presence of the excitation field components $\mu_0 h_x = \mu_0 h_y = 0.1$ mT. It can be seen that the spin-pumping current starts oscillating after the onset of the excitation field pulse and then damps out over the time scale of the magnetic damping. The excitation pulse width σ of the excitation field changes the envelope width of the resulting spin-current transient without affecting its amplitude or maximum (see Appendix A).

When the low AFMR mode is excited at $\Omega = \omega_l$, the out-of-plane linear spin current $I^{l,z}_{\rm sp}$ [blue line in Fig. 2(d)] dominates while the in-plane linear component $I^{l,x}_{\rm sp}$ has a much smaller amplitude [red line in Fig. 2(d)]. As for the nonlinear $\mathbf{I}^{\rm nl}_{\rm sp}$ shown in Fig. 2(g), it possesses a negligible magnitude (i.e., 6 orders of magnitude smaller than the linear counterpart) but an even higher oscillation frequency compared with the excitation field. On the other hand, at the high AFMR frequency $\Omega = \omega_h$, the in-plane $I^{l,x}_{\rm sp}$ [red line in Fig. 2(e)] is greatly enhanced and dominates over the out-of-plane counterpart $I^{l,z}_{\rm sp}$ [blue line in Fig. 2(e)]. This interchange of the relative amplitudes of the in-plane and out-of-plane components can be understood by recalling the previously defined factor $C_j = (m_{y1}/m_{z1})$. At $\Omega = \omega_l$ with the largely pronounced low AFMR mode, we have $|m_{y1}/m_{z1}| = |2i\mu_0\gamma' H_E/\omega_l| > 1$, since $\mu_0\gamma' H_E \sim$

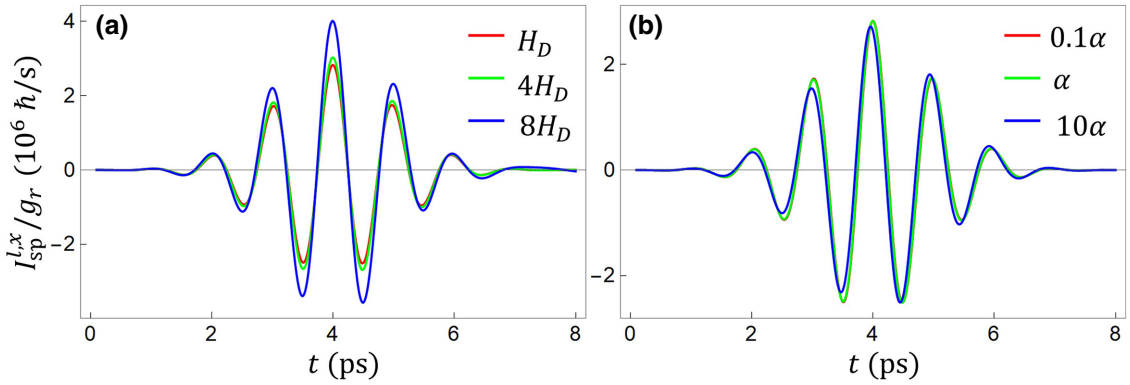

FIG. 3. The dominant in-plane linear spin-pumping current pulses $I_{sp}^{l,x}$ generated at THz frequencies (i.e., $\Omega = 2\pi \times 1$ THz) with different DMI fields (a) and different damping parameters (b). Other parameters are the same as in Fig. 2.

28 THz, i.e., the in-plane polarized magnetization component m_{y1} dominates. Considering $dm_{y1(z1)}/dt \propto i\omega_l m_{y1(z1)}$ under the pure harmonic excitation for simplicity, we obtain $dm_{y1(2)}/dt > dm_{z1(2)}/dt$ and therefore the corresponding linear spin current polarized along the out-of-plane direction (i.e., $I_{sp}^{l,z}$) would dominate [see Eq. (16)]. In the same way, the enhanced $I_{sp}^{l,x}$ at $\Omega = \omega_h$ can be explained by noting that $|m_{y1}/m_{z1}| = |i\omega_h/2\mu_0\gamma' H_E| < 1$. Such interchange of the relative amplitude of the in-plane and out-of-plane magnetization oscillation components between resonance and higher off-resonance frequencies has also been shown theoretically [29] and experimentally [30,31] in FM systems. Conversely, this amplitude exchange in AFM could be utilized to probe which AFMR mode dominates when both modes are excited at the same time, e.g., under excitation with $\mathbf{h} = (h_x, h_y)^T$ in our treatment.

Next, we turn to the investigation of the spin-pumping current in response to the excitation field at the much higher off-resonance THz regime. A coherent magnetization dynamics with a small amplitude has been detected in response to THz stimulus by time-resolved magneto-optical Kerr effect (MOKE) in FMs [31]. We also observe the generation of a coherent spin-pumping current transient at $\Omega = 2\pi \times 1$ THz for the canted AFM, as shown in Figs. 2(f) and 2(i). Although the magnitude of the dynamic magnetization (i.e., $\delta\mathbf{m}$) becomes very small in the off-resonance regime, the amplitude of the linear $\mathbf{I}_{sp}^{l}$ in Fig. 2(f) remains comparable with its resonant counterparts in Figs. 2(d) and 2(e). This is caused by the ultrafast temporal magnetization dynamics represented by the time derivative of $\delta\mathbf{m}$ that enters Eq. (16). In contrast, the nonlinear $\mathbf{I}_{sp}^{nl}$ in Eq. (17) contains both the dynamic magnetization $\delta\mathbf{m}$ and its time derivative, a competition between the enhanced temporal change of magnetization and the decreased magnetization amplitude in the THz regime. Figure 2(i) shows that the nonlinear $\mathbf{I}_{sp}^{nl}$ is 2 orders of magnitude smaller as compared with the resonance case. Note that the nonlinear components are much smaller than the linear components at both the resonant and THz regimes. In FMs, the in-plane $\mathbf{I}_{sp}^{l}$ under THz excitation is theoretically shown to be 2 orders of magnitude smaller than that of the resonant linear counterpart but comparable to the much smaller nonlinear $\mathbf{I}_{sp}^{nl}$ at resonance [29]. In contrast, AFM may provide a more efficient platform for THz spin-current pulse generation with comparable magnitude to that of the corresponding large linear resonant counterparts. Furthermore, the transient spin current can be excited at the higher off-resonance up to tens of THz with a sizable amplitude, which can be maintained at even higher frequencies beyond the THz regime. However, in the lower off-resonance regime (i.e., below the low AFMR frequency), the amplitude drops sharply and approaches zero. (See Appendix B for more details on the numerical results regarding these excitation frequencies.)

Now we focus on the in-plane linear spin current (i.e., $I_{sp}^{l,x}$), which dominates under the THz stimulus. Figure 3(a) shows the DMI dependence of $I_{sp}^{l,x}$. The spin current increases with a stronger DMI field H_D, consistent with the trend of the experimentally measured spin pumping signal based on the canted Fe_2O_3 heterostructure at the low AMFR mode under harmonic excitation [22]. Note that the DMI-induced enhancement at the off-resonance THz regime is lower than that of its resonant counterpart [21,22]. On the other hand, the sizable transient spin current at higher off-resonance can be also achieved in the absence of DMI, e.g., in a uniaxial or biaxial AFM. However, the presence of DMI would further enhance the signal amplitude. Our comprehensive model with DMI can be directly applied to collinear AFM systems without DMI by setting $H_D = 0$. In Fig. 3(b), we find that $I_{sp}^{l,x}$ has a negligible dependence on the damping constant α in the THz regime. However, the spin-pumping signal strongly depends on α at resonance (not shown here), as pointed out in our previous work [32]. This suggests that in evaluating the relative efficiency in generating

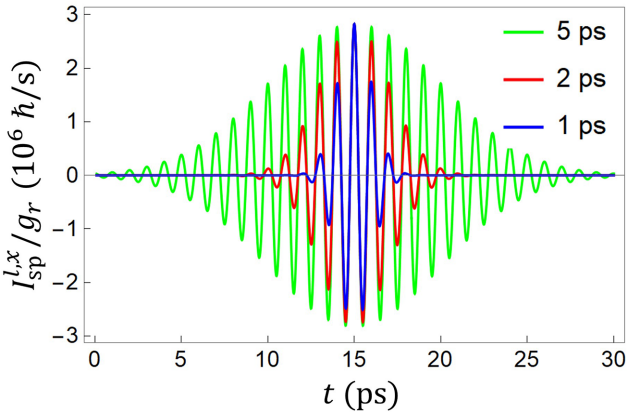

FIG. 4. The dominant in-plane linear spin-pumping current pulses $I_{sp}^{l,x}$ generated at $\Omega = 2\pi \times 1$ THz with different pulse widths. Other parameters are $\mu_0 h_x = \mu_0 h_y = 0.1$ mT, $\phi_h = 0$, and $t_0 = 15$ ns.

the coherent THz spin-pumping transient compared with its resonant counterparts, one has to factor in the damping parameter of the material for a valid comparison. In this work, we utilize the plausible parameter values (e.g., $\alpha = 4.6 \times 10^{-4}$) adapted from available experiments [21–25]. In addition, for uncompensated AFM/NM interfaces, the cross-sublattice damping and mixing conductance [33,34] can give rise to additional contributions to the spin-pumping transients, which are excluded in this work with compensated interface.

IV. CONCLUSION

In summary, we have developed an analytical model to calculate the spin pumping current transient excited by a THz pulse in canted AFM heterostructures. Surprisingly, we find strong coherent and pure spin-current transients generated at the higher off-resonance THz regime with comparable magnitude to the spin-pumping signal at resonance. This result is because the much smaller dynamic magnetization magnitude at off-resonance frequencies is compensated by the ultrafast change of the magnetic moments excited by the THz stimulus. Furthermore, we show that the DMI field enhances the magnitude of the spin-current transient. Our results suggest an efficient approach to generate coherent THz spin-current pulses based on canted AFM heterostructures without using a static magnetic field.

ACKNOWLEDGMENTS

This work is supported by the Ministry of Education (MOE) Tier-II grant MOE2018-T2-2-117 (NUS Grant No. R-263-000-E45-112/R-398-000-092-112) and MOE Tier-I FRC grant (NUS Grant No. R-263-000-D66-114). H.Y. is supported by the Agency for Science, Technology and Research (A*STAR) under its AME Individual Research Grants (A1983c0037) and National Research Foundation (NRF) Singapore Investigatorship (NRFI06-2020-0015). A.B. is supported by the Research Council of Norway through its Centres of Excellence funding scheme, project number 262633.

APPENDIX A: PULSE WIDTH DEPENDENCE

In this work, we consider a Gaussian pulse with different excitation frequencies, especially within the THz regime. Meanwhile, it is necessary to study the pulse width dependence with the frequency fixed. In Fig. 4, we plot the dominant in-plane linear spin-pumping current pulses $I_{sp}^{l,x}$ generated at $\Omega = 2\pi \times 1$ THz with different pulse widths. As expected, the pulse width σ of the excitation field changes the envelope width of the resulting spin-current transient without affecting its amplitude (maximum).

APPENDIX B: EXCITATION FREQUENCY RANGE

Based on the material parameters corresponding to canted Fe_2O_3, we obtain the two AFMR frequencies at

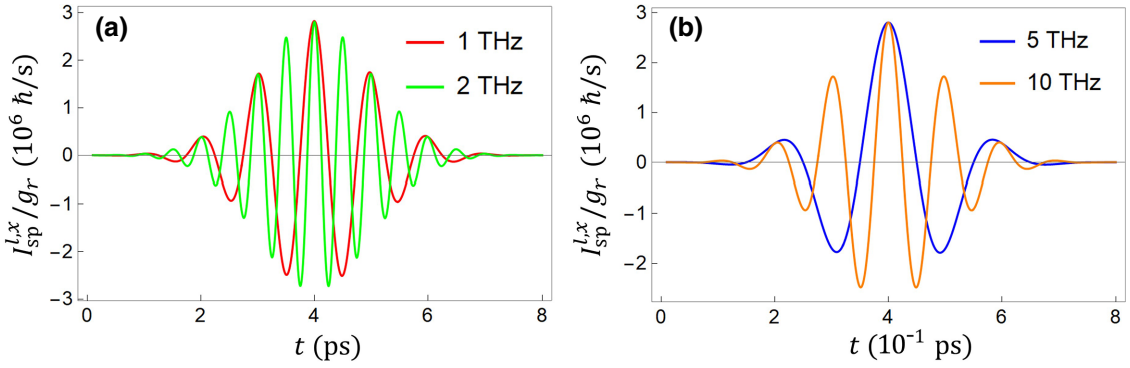

FIG. 5. The dominant in-plane linear spin-pumping current pulses $I_{sp}^{l,x}$ generated by different excitation frequencies within the higher off-resonance regime. The excitation field parameters of $\mu_0 h_x = \mu_0 h_y = 0.1$ mT and $\phi_h = 0$ are assumed. Other parameters are $\sigma = 1$ ps and $t_0 = 4$ ps (a) and $\sigma = 0.1$ ps and $t_0 = 0.4$ ps (b).

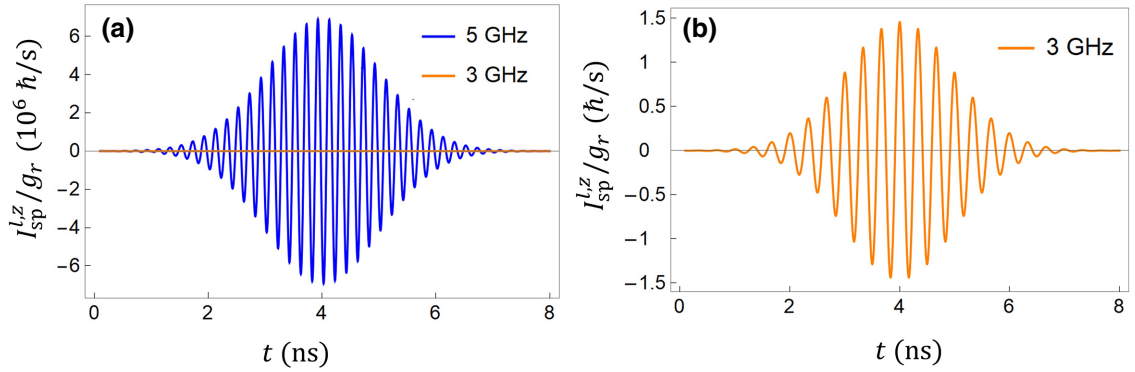

FIG. 6. (a) The dominant out-of-plane linear spin-pumping current pulses $I_{sp}^{l,z}$ generated by different excitation frequencies within the lower off-resonance regime. The excitation field parameters of $\mu_0 h_x = \mu_0 h_y = 0.1$ mT, $\phi_h = 0$, $\sigma = 1$ ns, and $t_0 = 4$ ns are assumed. (b) Enlarged diagram of $I_{sp}^{l,z}$ excited at 3 GHz in (a).

$\omega_l \sim 2\pi \times 9.7$ GHz and $\omega_h \sim 2\pi \times 85.1$ GHz. Here we investigate the spin-current transients under wider off-resonance frequency regime.

As described in the main text, the in-plane linear spin-current component $I_{sp}^{l,x}$ is greatly enhanced and dominates over the out-of-plane counterpart $I_{sp}^{l,z}$ at the high AFMR frequency ω_h (see Fig. 2). Therefore, we plot $I_{sp}^{l,x}$ at the higher off-resonance frequencies, as shown in Fig. 5. It can be seen that the spin-current signal maintains its large amplitude as the excitation frequency is further increased from 1 THz to much higher off-resonance frequencies up to 10 THz.

On the other hand, $I_{sp}^{l,z}$ dominates over $I_{sp}^{l,x}$ at the low AFMR frequency ω_l. Therefore, we plot $I_{sp}^{l,z}$ at the lower off-resonance frequencies in Fig. 6. Compared with the signal at the low AFMR resonance $\omega_l \sim 2\pi \times 9.7$ GHz [blue line in Fig. 2(d)], the spin current maintains a sizable amplitude when the excitation frequency is decreased to 5 GHz [blue line in Fig. 6(a)]. However, it drops sharply within the GHz region, i.e., it becomes 6 orders of magnitude smaller when the frequency is decreased to 3 GHz (orange line in Fig. 6).

[1] P. Sharma, How to create a spin current, Science **307**, 531 (2005).

[2] S. Maekawa, H. Adachi, K.-i. Uchida, J. i. Ieda, and E. Saitoh, Spin current: Experimental and theoretical aspects, J. Phys. Soc. Jpn. **82**, 102002 (2013).

[3] H. Zhao, E. J. Loren, H. Van Driel, and A. L. Smirl, Coherence Control of Hall Charge and Spin Currents, Phys. Rev. Lett. **96**, 246601 (2006).

[4] O. M. van't Erve, C. Awo-Affouda, A. T. Hanbicki, C. H. Li, P. E. Thompson, and B. T. Jonker, Information processing with pure spin currents in silicon: Spin injection, extraction, manipulation, and detection, IEEE Trans. Electron Devices **56**, 2343 (2009).

[5] S. Maekawa, S. O. Valenzuela, E. Saitoh, and T. Kimura, *Spin Current* (Oxford University Press, Oxford, UK, 2017), Vol. 22.

[6] C. Sun, J. Deng, S. Rafi-Ul-Islam, G. Liang, H. Yang, and M. B. Jalil, Field-Free Switching of Perpendicular Magnetization Through Spin Hall and Anomalous Hall Effects in Ferromagnet–Heavy-Metal–Ferromagnet Structures, Phys. Rev. Appl. **12**, 034030 (2019).

[7] J. Walowski and M. Münzenberg, Perspective: Ultrafast magnetism and THz spintronics, J. Appl. Phys. **120**, 140901 (2016).

[8] G.-M. Choi, B.-C. Min, K.-J. Lee, and D. G. Cahill, Spin current generated by thermally driven ultrafast demagnetization, Nat. Commun. **5**, 4334 (2014).

[9] T. Kampfrath, M. Battiato, P. Maldonado, G. Eilers, J. Nötzold, S. Mährlein, V. Zbarsky, F. Freimuth, Y. Mokrousov, S. Blügel, M. Wolf, I. Radu, P. M. Oppeneer, and M. Münzenberg, Terahertz spin current pulses controlled by magnetic heterostructures, Nat. Nanotechnol. **8**, 256 (2013).

[10] Y. Wu, M. Elyasi, X. Qiu, M. Chen, Y. Liu, L. Ke, and H. Yang, High-performance THz emitters based on ferromagnetic/nonmagnetic heterostructures, Adv. Mater. **29**, 1603031 (2017).

[11] M. Chen, R. Mishra, Y. Wu, K. Lee, and H. Yang, Terahertz emission from compensated magnetic heterostructures, Adv. Opt. Mater. **6**, 1800430 (2018).

[12] T. Seifert, *et al.*, Efficient metallic spintronic emitters of ultrabroadband terahertz radiation, Nat. Photonics **10**, 483 (2016).

[13] C. Sun, S. Rafi-Ul-Islam, H. Yang, and M. B. Jalil, Spin Nernst and anomalous Nernst effects and their signature outputs in ferromagnet/nonmagnet heterostructures, Phys. Rev. B **102**, 214419 (2020).

[14] Y. Tserkovnyak, A. Brataas, and G. E. Bauer, Spin pumping and magnetization dynamics in metallic multilayers, Phys. Rev. B **66**, 224403 (2002).

[15] B. Heinrich, C. Burrowes, E. Montoya, B. Kardasz, E. Girt, Y.-Y. Song, Y. Sun, and M. Wu, Spin Pumping at the Magnetic Insulator (YIG)/Normal Metal (Au) Interfaces, Phys. Rev. Lett. **107**, 066604 (2011).

[16] S. Rezende, R. Rodríguez-Suárez, M. Soares, L. Vilela-Leão, D. Ley Domínguez, and A. Azevedo, Enhanced spin pumping damping in yttrium iron garnet/Pt bilayers, Appl. Phys. Lett. **102**, 012402 (2013).

[17] V. Castel, N. Vlietstra, B. Van Wees, and J. B. Youssef, Frequency and power dependence of spin-current emission by spin pumping in a thin-film YIG/Pt system, Phys. Rev. B **86**, 134419 (2012).

[18] M. Haertinger, C. H. Back, J. Lotze, M. Weiler, S. Geprägs, H. Huebl, S. T. Gönnenwein, and G. Woltersdorf, Spin pumping in YIG/Pt bilayers as a function of layer thickness, Phys. Rev. B **92**, 054437 (2015).

[19] J. Li, C. B. Wilson, R. Cheng, M. Lohmann, M. Kavand, W. Yuan, M. Aldosary, N. Agladze, P. Wei, M. S. Sherwin, and J. Shi, Spin current from sub-terahertz-generated antiferromagnetic magnons, Nature **578**, 70 (2020).

[20] P. Vaidya, S. A. Morley, J. van Tol, Y. Liu, R. Cheng, A. Brataas, D. Lederman, and E. Del Barco, Subterahertz spin pumping from an insulating antiferromagnet, Science **368**, 160 (2020).

[21] I. Boventer, H. Simensen, A. Anane, M. Kläui, A. Brataas, and R. Lebrun, Room-Temperature Antiferromagnetic Resonance and Inverse Spin-Hall Voltage in Canted Antiferromagnets, Phys. Rev. Lett. **126**, 187201 (2021).

[22] H. Wang, Y. Xiao, M. Guo, E. Lee-Wong, G. Q. Yan, R. Cheng, and C. R. Du, Spin Pumping of an Easy-Plane Antiferromagnet Enhanced by Dzyaloshinskii–Moriya Interaction, Phys. Rev. Lett. **127**, 117202 (2021).

[23] C. Searle and S. Wang, Magnetic-resonance properties of pure and titanium-doped hematite, J. Appl. Phys. **39**, 1025 (1968).

[24] R. Lebrun, A. Ross, O. Gomonay, S. A. Bender, L. Baldrati, F. Kronast, A. Qaiumzadeh, J. Sinova, A. Brataas, R. A. Duine, and M. Kläu, Anisotropies and magnetic phase transitions in insulating antiferromagnets determined by a Spin-Hall magnetoresistance probe, Commun. Phys. **2**, 1 (2019).

[25] H. Fink, Resonance line shapes of weak ferromagnets of the α-Fe_2O_3 and NiF_2 type, Phys. Rev. **133**, A1322 (1964).

[26] L. Bocklage, Transient magnetization dynamics in the free energy formulation of the landau-lifshitz equation, J. Magn. Magn. Mater. **429**, 324 (2017).

[27] L. Bocklage, Model of THz magnetization dynamics, Sci. Rep. **6**, 1 (2016).

[28] R. Cheng, J. Xiao, Q. Niu, and A. Brataas, Spin Pumping and Spin-Transfer Torques in Antiferromagnets, Phys. Rev. Lett. **113**, 057601 (2014).

[29] L. Bocklage, Coherent THz Transient Spin Currents by Spin Pumping, Phys. Rev. Lett. **118**, 257202 (2017).

[30] L. Bocklage, C. Swoboda, K. Schlage, H.-C. Wille, L. Dzemiantsova, S. Bajt, G. Meier, and R. Röhlsberger, Spin Precession Mapping at Ferromagnetic Resonance via Nuclear Resonant Scattering of Synchrotron Radiation, Phys. Rev. Lett. **114**, 147601 (2015).

[31] C. Vicario, C. Ruchert, F. Ardana-Lamas, P. M. Derlet, B. Tudu, J. Luning, and C. P. Hauri, Off-resonant magnetization dynamics phase-locked to an intense phase-stable terahertz transient, Nat. Photonics **7**, 720 (2013).

[32] C. Sun, H. Yang, and M. B. Jalil, Ferrimagnetic resonance induced by the spin Hall effect, Phys. Rev. B **102**, 134420 (2020).

[33] A. Kamra, R. E. Troncoso, W. Belzig, and A. Brataas, Gilbert damping phenomenology for two-sublattice magnets, Phys. Rev. B **98**, 184402 (2018).

[34] R. E. Troncoso, M. A. Lund, A. Brataas, and A. Kamra, Cross-sublattice spin pumping and magnon level attraction in van der Waals antiferromagnets, Phys. Rev. B **103**, 144422 (2021).